INTERNATIONAL JOURNAL FOR NUMERICAL METHODS IN FLUIDS
Int. J. Numer. Meth. Fluids 2005; **47**:575–589
Published online 22 December 2004 in Wiley InterScience (www.interscience.wiley.com). DOI: 10.1002/fld.832

Parallel finite element simulation for orographic wind flow and rainfall using GIS data

Kazuo Kashiyama*,†, Takahiro Shimizu, Tetsuhiro Kurahashi and Hidetaka Hamada

Department of Civil Engineering, Chuo University, 1-13-27 Kasuga, Bunkyo-ku, Tokyo 112-8551, Japan

SUMMARY

This paper presents a computational technique based on the finite element method for the orographic wind flow and rainfall. The governing equations are the unsteady Navier–Stokes equations based on Boussinesq approximation and the Kessler model for warm rain. The SUPG/PSPG method is employed for the stabilization method. The automatic mesh generation method using GIS data is utilized to develop an accurate geographic model. The present method is applied to the analysis of orographic wind flow and rainfall past a semicircular hill and an actual mountain area. Copyright © 2004 John Wiley & Sons, Ltd.

KEY WORDS: stabilized FEM; orographic wind flow and rainfall; PC cluster; mesh generation; GIS

1. INTRODUCTION

A number of natural disasters due to wind and rainfall occur annually in various parts of the world. In order to estimate the extent of a disaster quantitatively, it is necessary to estimate the wind flow and rainfall. Rainfall can be classified into two types: orographic and convective rainfall. Orographic rainfall is caused by the clouds produced by ascending wind flow due to the ups and downs of geological features. On the other hand, convective rainfall is caused by the clouds produced by ascending wind flow due to instability of the air layers. Some physical models for these types of rainfall have been presented in the past [1–5]. The models are classified in warm rain [1, 2] and cold rain [3–5] whether the model includes the effect of ice and snow. In the previous studies, Tateya *et al.* [2] presented a numerical method based on the finite difference method for the analysis of orographic rainfall for warm rain. The Kessler model [1] was used as the governing

*Correspondence to: Kazuo Kashiyama, Department of Civil Engineering, Chuo University, 1-13-27 Kasuga, Bunkyo-ku, Tokyo 112-8551, Japan.
†E-mail: kaz@civil.chuo-u.ac.jp

Contract/grant sponsor: Scientific Research of the Japan Society; contract/grant numbers: 12650482, 12555136

Received 5 January 2004
Accepted 18 August 2004

equation for warm rain and the potential flow theory was applied to the governing equations of wind flow.

This paper presents a numerical method based on the parallel finite element method for the analysis of orographic wind flow and rainfall in order to improve the applicability of the numerical simulation method. The Kessler model is used as the governing equation for warm rain. It represents the conservation equations of cloud and rainwater content. On the other hand, the unsteady Navier–Stokes equation based on Boussinesq approximation is used for the governing equations of wind flow. The SUPG/PSPG (pressure-stabilizing/Petrov–Galerkin) [6, 7] finite element method is used for solving wind flows. The SUPG (streamline-upwind/Petrov–Galerkin) method is employed for solving the cloud and rainwater equations. The P1/P1 element (linear interpolation, both for velocity and pressure) is employed for the discretization in space. The algebraic equations resulting from the finite element discretization are solved using the element-by-element Bi-CGSTAB2 method. Computations are carried out on a PC cluster [8]. The parallel implementation is based on domain decomposition method and utilizes MPI libraries. In this type of computations, it is important that the finite element mesh accurately represent the details of geographical features. Therefore, the automatic mesh generation method using GIS data was also developed. The Delaunay method was employed for generating the finite element mesh. In order to express the geographical features accurately, the valley and mountain lines are represented as an edge of the finite element. The present simulation method is applied to the analysis of orographic wind flow and rainfall past a semicircular hill and an actual mountain area. The computed results are compared with the experimental results. The effect of parallelization on the efficiency of the computation is also examined.

2. BASIC EQUATION

Assuming that the air is viscous incompressible and Newtonian fluid, the wind flow can be described by the Navier–Stokes equation based on Boussinesq approximation.

$$\dot{u_i} + u_j u_{i,j} + \frac{1}{\rho_0} p_{,i} - \nu(u_{i,jj} + u_{j,ij}) + \frac{\rho}{\rho_0} g\delta_{i3} = 0 \tag{1}$$

$$u_{i,i} = 0 \tag{2}$$

$$\dot{\rho} + u_i \rho_{,i} = -\rho_z u_i \delta_{i3} \tag{3}$$

where u_i is the velocity, p is the pressure, ρ_0 is the reference density, ρ is the gap to the reference density, ρ_z is the vertical gradient of the density, ν is the viscosity of fluid and δ_{ij} is the Kronecker's delta.

The Dirichlet and Neumann type boundary conditions are given as follows:

$$u_i = g_i \quad \text{on } \Gamma_g \tag{4}$$

$$n_j \left(-\frac{1}{\rho_0} p\delta_{ij} + \nu \left(u_{i,j} + u_{j,i} \right) \right) = h_i \quad \text{on } \Gamma_h \tag{5}$$

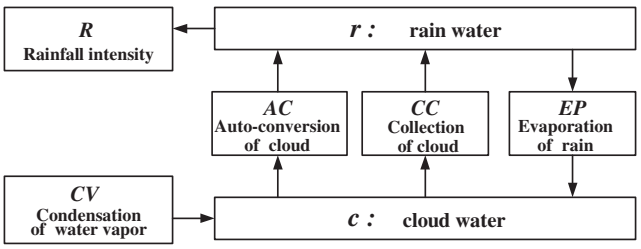

Figure 1. Kessler model.

The Kessler model for warm rain is used for the governing equation. Figure 1 shows the schematic description of the rainfall mechanism according to the Kessler model [1]. The governing equations represent the conservation laws for cloud and rain water content:

$$\dot{c} + u_i c_{,i} = -\mathrm{AC} - \mathrm{CC} + \mathrm{EP} + \mathrm{CV} \tag{6}$$

$$\dot{r} + (u_i + W\delta_{i3}) r_{,i} = \mathrm{AC} + \mathrm{CC} - \mathrm{EP} \tag{7}$$

Here, c is the cloud water content, r is the rainwater content in the air, u_i is the wind velocity, W is the falling speed of raindrops, AC, CC, EP and CV are the terms representing auto-conversion of clouds, collection of clouds, evaporation of rain and condensation of water vapour, respectively. The effect of vertical temperature distribution is included in the term of condensation of water vapour. The cloud water content can be expressed as

$$c = q - Q_{\mathrm{S}} \tag{8}$$

where q is the water vapour content and Q_{S} is the saturated water vapour content in the air. Therefore, $c = 0$ corresponds to a saturated air–water mixture.

The falling speed of raindrops is assumed to follow the relation:

$$W = -38.3 N_0^{-1/8} \cdot r^{1/8} \exp(kz/2) \tag{9}$$

where N_0 is the Marshall–Palmer constant($= 10^7\,\mathrm{m}^{-4}$), k is the lapse rate of air density ($= 10^{-4}\,\mathrm{m}^{-1}$) and z is the altitude (m).

The rainfall intensity R (mm/h) is related to the rainwater content as

$$R = 138 N_0^{-1/8} \cdot r^{9/8} \tag{10}$$

The Dirichlet type boundary condition corresponding to Equations (6) and (7) is given as

$$c = g, \quad r = g \quad \text{on } \Gamma_g \tag{11}$$

3. FINITE ELEMENT DISCRETIZATION

For the discretization in space, the stabilized finite element method based on the SUPG (streamline upwind/Petrov–Galerkin) and PSPG (pressure stabilized/Petrov–Galerkin) method

[6, 7] is employed for the Navier–Stokes equation. The weak form of Equations (1) and (2) can be expressed as follows:

$$\int_\Omega w_i(\dot{u_i} + u_j u_{i,j})\,\mathrm{d}\Omega - \int_\Omega w_{i,i}\,\frac{1}{\rho_0}\,p\,\mathrm{d}\Omega + \int_\Omega w_{i,j}\nu(u_{i,j}+u_{j,i}) + \int_\Omega q u_{i,i}\,\mathrm{d}\Omega + \int_\Omega w_i\,\frac{\rho}{\rho_0}\,g\delta_{i3}\,\mathrm{d}\Omega + \sum_{e=1}^{n_{\mathrm{el}}}\int_{\Omega^e}\{\tau_{\mathrm{supg1}}u_k w_{i,k} + \tau_{\mathrm{pspg}}q_{,i}\}\left\{\dot{u_i} + u_j u_{i,j} + \frac{1}{\rho_0}\,p_{,i} - \nu(u_{i,jj}+u_{j,ij}) + \frac{\rho}{\rho_0}\,g\delta_{i3}\right\}\mathrm{d}\Omega = \int_\Gamma w_i h_i\,\mathrm{d}\Gamma \tag{12}$$

where w_i and q denote weighting functions. The first five integrals are Galerkin terms and the series of element-level integral is the term due to SUPG/PSPG stabilization.

For the discretization of the density equation and the conservation equations of cloud water content and rainwater content, the stabilized finite element method based on the SUPG method is employed as follows:

$$\int_\Omega w(\dot{\rho} + u_i\rho_{,i} + \rho_z u_i\delta_{i3})\,\mathrm{d}\Omega + \sum_{e=1}^{n_{\mathrm{el}}}\int_{\Omega^e}\tau_{\mathrm{supg2}}u_j w_{,j}(\dot{\rho} + u_i\rho_{,i} + \rho_z u_i\delta_{i3})\,\mathrm{d}\Omega = 0 \tag{13}$$

$$\int_\Omega w(\dot{c} + u_i c_{,i} - f_c)\,\mathrm{d}\Omega + \sum_{e=1}^{n_{\mathrm{el}}}\int_{\Omega^e}\tau_{\mathrm{supg2}}u_j w_{,j}(\dot{c} + u_i c_{,i} - f_c)\,\mathrm{d}\Omega = 0 \tag{14}$$

$$\int_\Omega w(\dot{r} + \bar{u}_i r_{,i} - f_r)\,\mathrm{d}\Omega + \sum_{e=1}^{n_{\mathrm{el}}}\int_{\Omega^e}\tau_{\mathrm{supg2}}\bar{u}_j w_{,j}(\dot{r} + \bar{u}_i r_{,i} - f_r)\,\mathrm{d}\Omega = 0 \tag{15}$$

In Equations (13)–(15), the first integral is the Galerkin term. The series of element-level integral is the SUPG term: $\bar{u}_i$ is the wind velocity considering the fall speed of raindrops ($\bar{u}_i = u_i + W\delta_{i3}$), f_c and f_r denote source term. The stabilization parameters τ_{supg1}, τ_{pspg} and τ_{supg2} are defined as follows:

$$\tau_{\mathrm{supg1}} = \left[\left(\frac{2}{\Delta t}\right)^2 + \left(\frac{2\|u_i\|}{h_e}\right)^2 + \left(\frac{4\nu}{h_e^2}\right)^2\right]^{-1/2} \tag{16}$$

$$\tau_{\mathrm{pspg}} = \tau_{\mathrm{supg1}} \tag{17}$$

$$\tau_{\mathrm{supg2}} = \left[\left(\frac{2}{\Delta t}\right)^2 + \left(\frac{2\|u_i\|}{h_e}\right)^2\right]^{-1/2} \tag{18}$$

where Δt is the time increment and h_e is the element length.

Using the P1/P1 element (linear interpolation both for velocity and pressure) for the discretization in space, the following finite element equations are obtained.

$$(\mathbf{M}+\mathbf{M}_\delta)\dot{u_i}+(\mathbf{K}(u_j)+\mathbf{K}_\delta(u_j))u_i-(\mathbf{C}-\mathbf{C}_\delta)\frac{1}{\rho_0}p+\nu\mathbf{S}u_i+(\mathbf{M}+\mathbf{M}_\delta)\frac{\rho}{\rho_0}g\delta_{i3}=0 \quad (19)$$

$$\mathbf{C}^{\mathrm{T}}u_i+\mathbf{M}_\varepsilon\dot{u_i}+\mathbf{K}_\varepsilon(u_j)u_i+\mathbf{C}_\varepsilon\frac{1}{\rho_0}p+\mathbf{M}_\varepsilon\frac{\rho}{\rho_0}g\delta_{i3}=0 \quad (20)$$

$$(\mathbf{M}+\mathbf{M}_\delta)\dot{\rho}+(\mathbf{K}(u_i)+\mathbf{K}_\delta(u_i))\rho+(\mathbf{M}+\mathbf{M}_\delta)\rho_z u_i\delta_{i3}=0 \quad (21)$$

$$(\mathbf{M}+\mathbf{M}_\delta)\dot{c}+(\mathbf{K}(u_i)+\mathbf{K}_\delta(u_i))c-(\mathbf{M}+\mathbf{M}_\delta)f_c=0 \quad (22)$$

$$(\mathbf{M}+\mathbf{M}_\delta)\dot{r}+(\mathbf{K}(\bar{u}_i)+\mathbf{K}_\delta(\bar{u}_i))r-(\mathbf{M}+\mathbf{M}_\delta)f_r=0 \quad (23)$$

where, **M**, **K**, **C** and **S** are the coefficient matrices derived from each term of the weak form. The subscripts δ and ε denote the SUPG and PSPG contributions, respectively.

The implicit scheme based on the Crank–Nicolson technique is employed for the temporal discretization of Equations (19)–(23). To solve the simultaneous equation, the element-by-element BiCGSTAB2 method is applied. The solution procedure is shown in Figure 2.

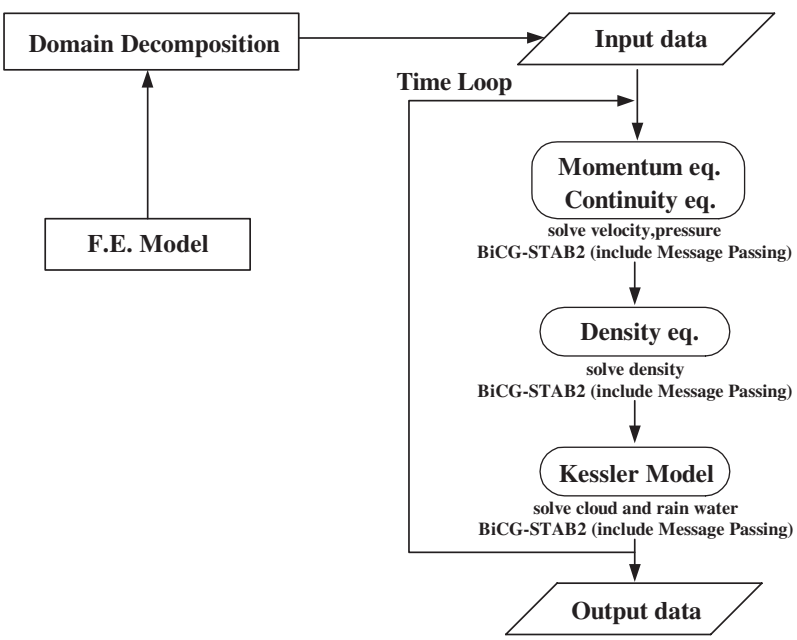

Figure 2. Flow chart.

Table I. Specifications of a component computer of the PC cluster.

PC cluster parallel computer (20PCs)	
CPU	Intel-Xeon
Clock cycle	3.06 GHz
Cache size	1 MB
Memory size	2 GB
O.S.	Red-Hat Linux 7.3
Network	1000Base-T

4. PARALLEL IMPLEMENTATION

A parallel computational scheme based on the domain decomposition method [9, 10] was developed in order to reduce the CPU time and computer storage required. A parallel implementation using the MPI libraries suitable for unstructured grid was designed for use on a PC cluster [8]. The PC cluster consists of 20 nodes, each with an Intel-Xeon 3.06 GHz processor and 2GB memory. The giga-bit ethernet (1000Base-T network) and a switching hub are employed for the network environment. Table I shows the specifications of a component computer of the PC cluster. The MPICH-SCore was used for MPI and PGI Fortran was used for compiling the source codes. The automatic mesh decomposer, METIS [10], based on the multilevel k-way partitioning scheme [9] was employed to minimize the amount of interprocessor communication. For each sub-domain, the processor associated with that sub-domain carries out computations independently.

The element-by-element Bi-CGSTAB2 method was employed to solve the finite element equations. The parallel implementation results in a quick and efficient solution to the resulting equation systems. The parallel implementation requires two types of communications. The communication between neighbour processors is needed for the assembly of element level vector and that among all the processors is needed for the calculation of residual norm.

5. MESH GENERATION USING GIS DATA

In order to generate a finite element mesh that accurately represents the details of geographical features, an automatic mesh generation method using GIS data was developed. For the data of land elevation, the digital elevation map issued by the Japanese geographical survey institute was employed. The resolution of the map was 50 m. The Arc View software [11, 12] was used for the GIS system. Figure 3 shows the contour line for Miyake Island in Japan. In order to obtain the information of ridge and valley lines, a finer grid which is called the grid surface was prepared and the elevation of the grid points are interpolated by the 3rd order spline function. The grid size was assumed to be 10 m. Applying the analysis of the direction of stream using the grid surface, the ridge and valley lines can be obtained as in Figure 4. The nodal points were generated on the ridge and valley lines at the constant interval. The Delaunay method [13] was utilized for generating the finite element mesh. In order to express the geographical features accurately, the ridge and valley lines were expressed as an edge of the finite element. Figure 5 shows the surface mesh for Miyake Island. From this figure,

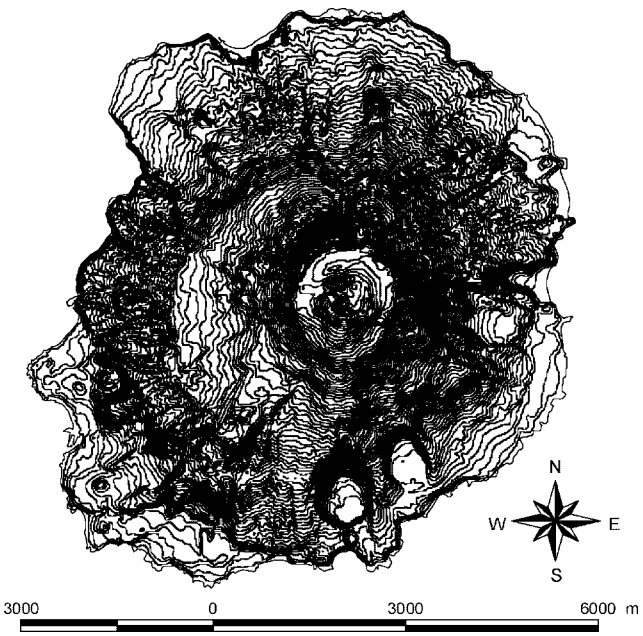

Figure 3. Contour line for Miyake Island.

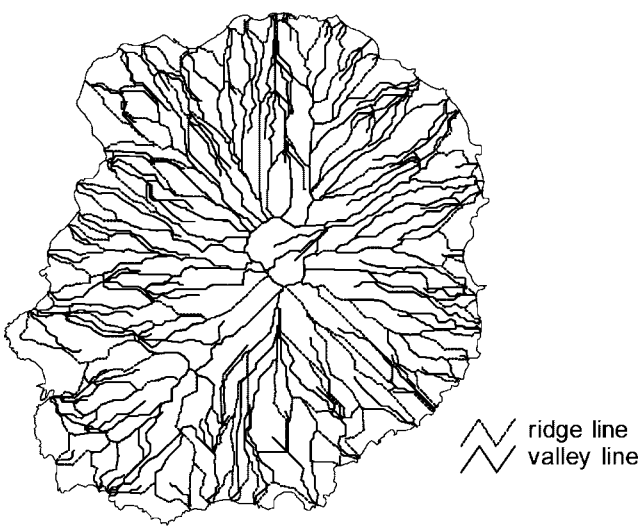

Figure 4. Ridge and valley line for Miyake Island.

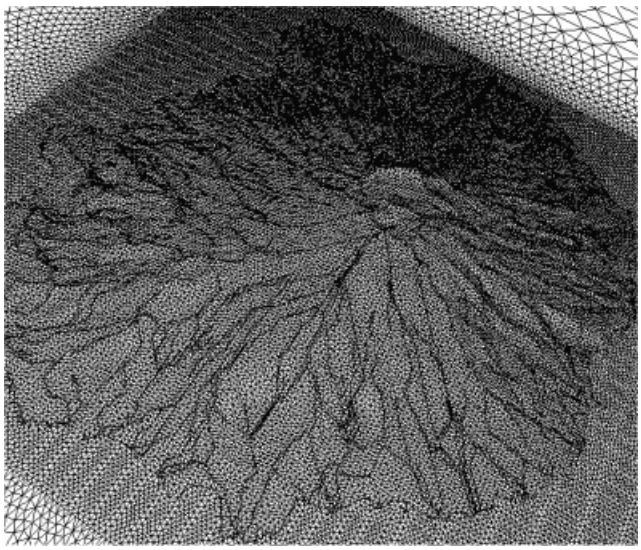

Figure 5. Finite element mesh for ground surface.

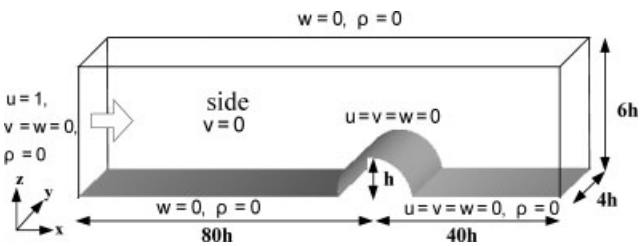

Figure 6. Boundary condition.

it can be seen that the finite element model expresses the geometrical features accurately. The unstructured tetrahedral mesh was generated for the 3-D domain using the surface mesh described above.

6. NUMERICAL EXAMPLES

The present method is applied to the wind flow past a semicircular hill [14]. The 2-D and 3-D analysis is performed to check the validity of the method. The computational domain and boundary conditions are illustrated in Figure 6. The span length is assumed to be $4h$, where h is the height of a semicircular hill. In this example, the non-dimensional equation system is employed. The Reynolds number is assumed to be 2000. The computation is carried out using different values of the degree of air-density stratification. The total number of elements and nodes are 28,424 and 14,611 in the case of 2-D analysis and 241,920 and 57,827 in the case

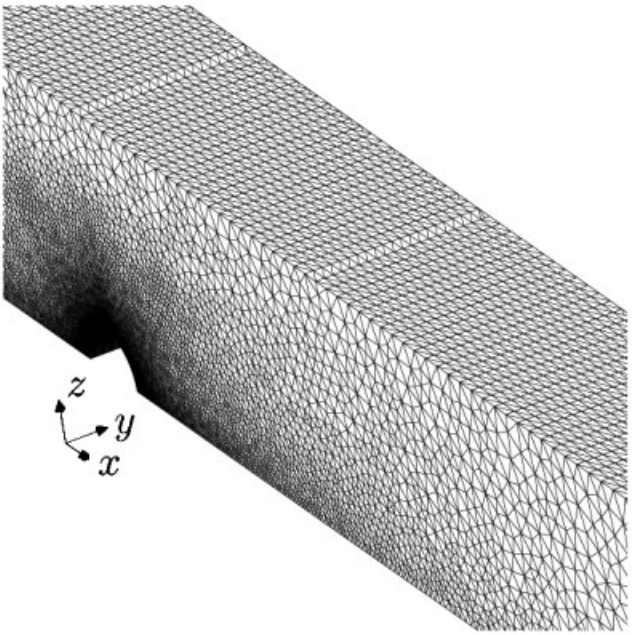

Figure 7. Finite element idealization.

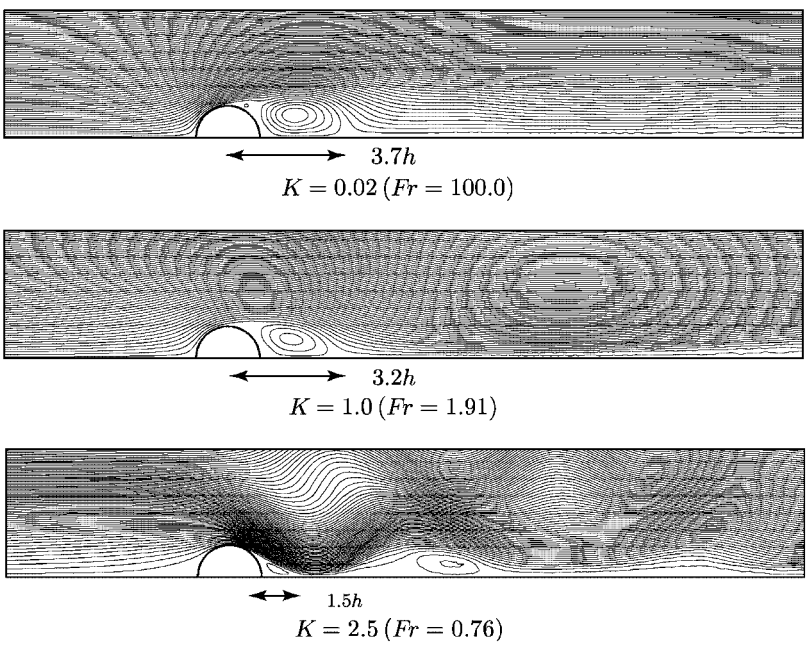

Figure 8. Computed mean streamline for 2D analysis.

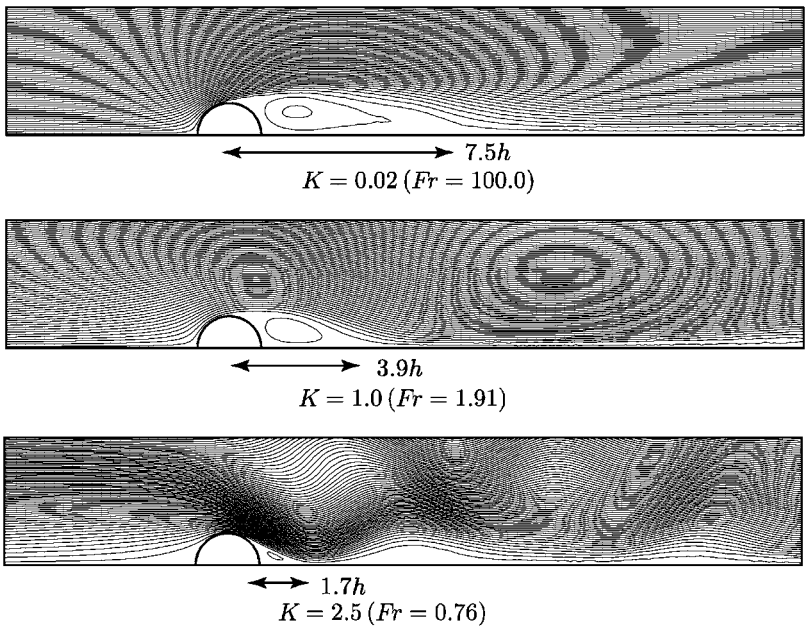

Figure 9. Computed mean streamline for 3D analysis.

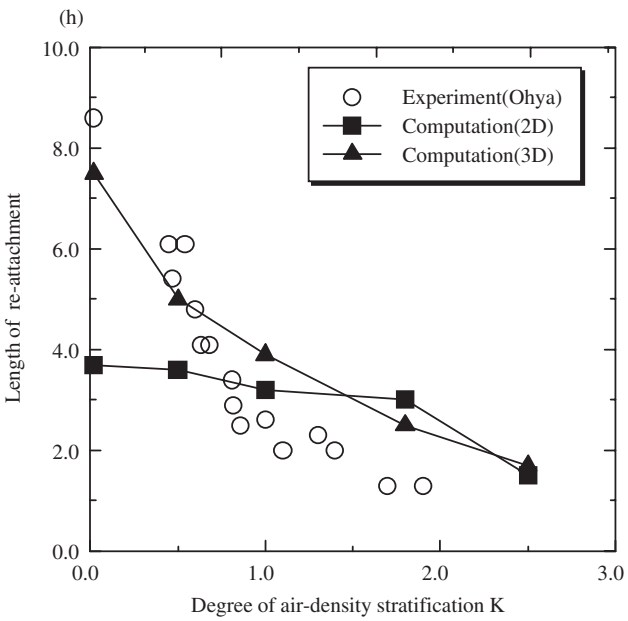

Figure 10. Comparison with computed and experimental results for the length of re-attachement of streamline.

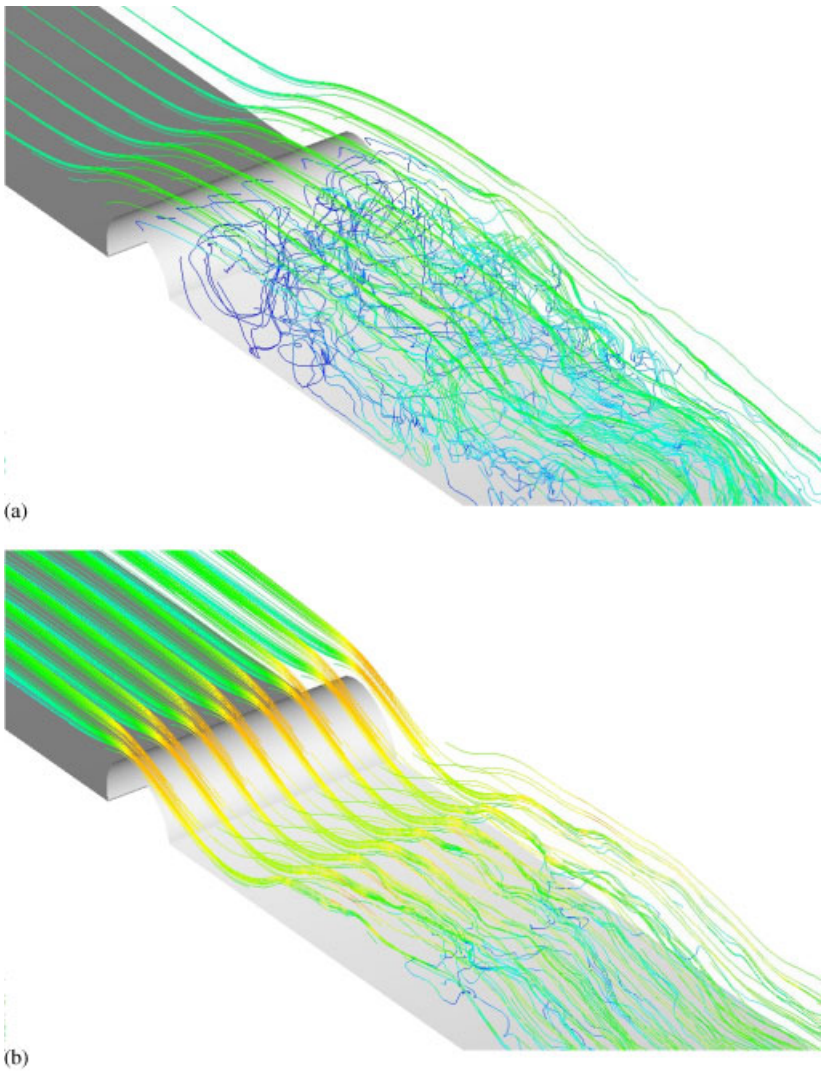

Figure 11. Computed streamline at $t = 120$.

of 3-D analysis, respectively. Figure 7 shows the finite element mesh around a semicircular hill for the 3-D analysis. The finite element mesh for the 2-D analysis is the same as the 3-D mesh for the vertical x–z section shown in Figure 7. The time increment is assumed to be $\Delta t = 0.001$. Figures 8 and 9 show the 2-D and 3-D results of mean streamline versus the degree of air-density stratification K (or the Froude Number Fr). From these results, the effect of air-density stratification can be clearly seen. The length of re-attachment of the streamline becomes shorter with the increase in the degree of air-density stratification. Figure 10 shows the comparison of the length of re-attachment versus the degree of air-density stratification between numerical and experimental results [14]. The numerical result obtained by the 3-D

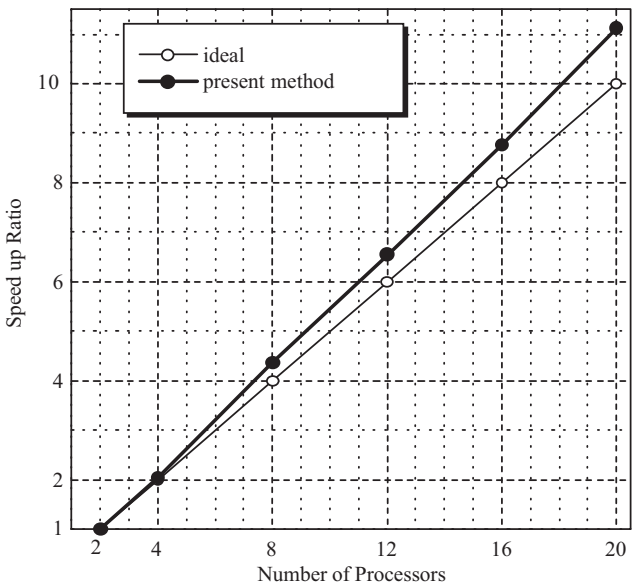

Figure 12. Speed-up ratio versus number of processors.

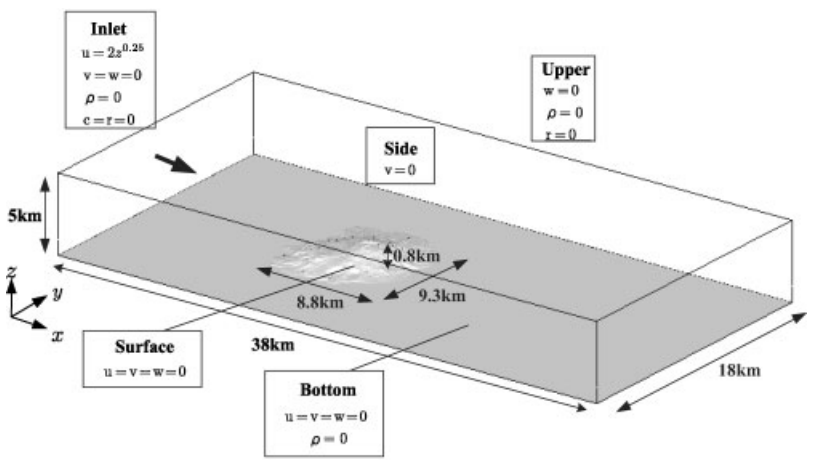

Figure 13. Boundary condition for orographic windflow and rainfall for Miyake Island.

analysis is in good agreement with the experimental results. Figure 11 shows the computed streamline at $t = 120$ in case of $K = 0.02$ ($Fr = 100$) and $K = 2.5$ ($Fr = 0.76$). From this figure, it can be seen that the three-dimensional effects are stronger when the degree of air density stratification is low. This is the reason why the numerical results obtained by the 2-D analysis are not in agreement with the experimental results. Figure 12 shows the speed-up ratio versus the number of processors in the case of 3-D analysis. It can be seen that the super-linear parallel performance was obtained by the effect of cache memory.

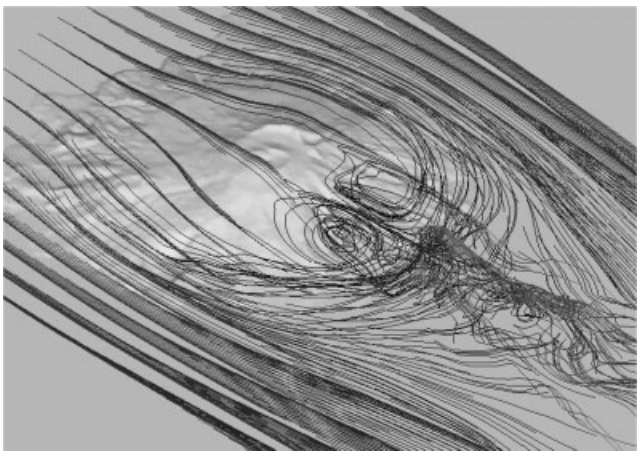

Figure 14. Computed streamline which starts from the elevation level 250 m at $t = 3$ h.

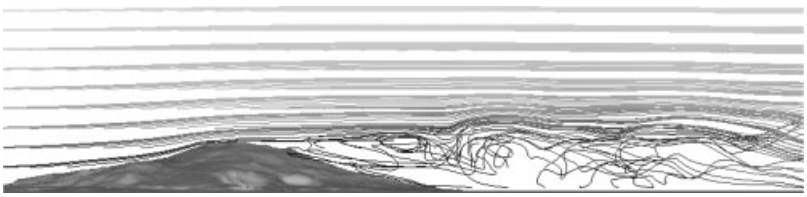

Figure 15. Computed streamline at $t = 3$ h.

Figure 16. Computed cloud water content at $t = 3$ h.

The present method was applied to the actual mountain area shown in Figure 13. The vertical length of computational domain was assumed to be 5 km, where the height of Miyake Island is about 800 m. The Reynolds number and the time increment are $R_e = 2000$ and $\Delta t = 0.5$ s, respectively. Figure 14 shows the computed streamline, which starts from the elevation level 250 m at time $t = 3$ h. From this figure, it can be seen that the twin vortices are located behind the mountain. Figures 15–17 show the computed streamline, cloud and rainwater content respectively, at the central section of the island at time $t = 3$ h. From these figures, it can be seen that the cloud water and rainwater generated by the ascending wind flow due to the slope of the mountain are transposed to the downstream side. Figure 18 shows the time history of the rain intensity at points A, B, C and D shown in Figure 17. From this figure, it is seen that strong rains occur behind the mountain and the rain intensity at points

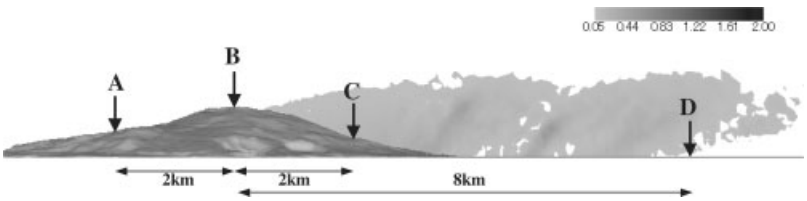

Figure 17. Computed rainwater content at $t = 3$ h.

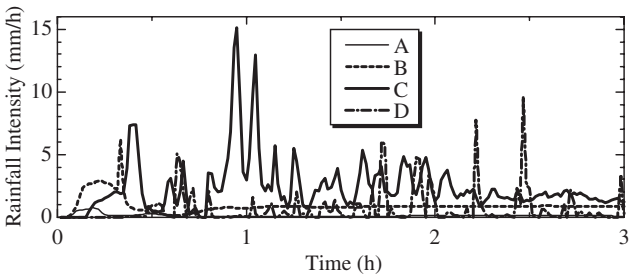

Figure 18. Computed rain intensity at points A, B, C and D.

C and D fluctuates due to the advection of cloud and rainwater. The computational results are in agreement with the actual rain phenomena, qualitatively.

7. CONCLUSIONS

A simulation method based on parallel finite element method for the analysis of orographic wind flow and rainfall has been presented. The Navier–Stokes equation, based on Boussinesq approximation, and the Kessler model were employed for the governing equations. The stabilized finite element method based on SUPG/PSPG method was employed. The parallel implementation based on domain decomposition and MPI was designed for the use of PC cluster parallel computer. The automatic mesh generation method using GIS data was also developed to generate a finite element mesh that accurately expresses the details of geographical features. The computed results obtained by the present method were in agreement with the experimental results and actual phenomena, qualitatively. Good parallel performance was obtained using a PC cluster. The verification of the method of rainfall analysis will be presented in a future work.

ACKNOWLEDGEMENTS

This research was supported by the grant-in-aid for Scientific Research of the Japan society for the Promotion of Science, No.12650482 and No.12555136.

REFERENCES

1. Kessler E. Models of microphysical parameters and processes. *Meteorological Monographs* 1969; **10**:26–31.
2. Tateya K, Nakatsugawa M, Yamada T. Investigation of rainfall by field observations and a physically based model. *Proceedings of Pacific International Seminar on Water Resources System* 1989; 385–403.
3. Steven AR, Hobbs PV. The mesoscale and microscale structure and organization of clouds and precipitation in midlatitude cyclones. *Journal of Atmospheric Sciences* 1983; **40**:1185–1206.
4. Yamada T, Hibino T, Matsuura M. Numerical simulation of precipitation considering cloud microphysics. *Proceedings of 25th Congress of IAHR*, 1993; 1127–1134.
5. Yamada T, Ikenaga H, Saka N, Saito D, Matsuura T. Numerical simulation of orographic rainfall considering cloud microphysical processes and aerosols. *Proceedings of Pacific International Conference on Water Resources and Environmental Research*, 1996; 197–204.
6. Tezduyar TE. Stabilized finite element formulations for incompressible flow computations. *Advances in Applied Mechanics* 1991; **28**:1–44.
7. Tezduyar TE, Mittal S, Ray SE, Shih R. Incompressible flow computations with stabilized bilinear and linear equal-order-interpolation velocity-pressure elements. *Computer Methods Applied Mechanics and Engineering* 1992; **95**:221–242.
8. Kashiyama K, Tanaka S, Sakuraba M. PC cluster parallel finite element analysis of sloshing problem by earthquake using different network environments. *Communications in Numerical Methods in Engineering* 2002; **18**:681–690.
9. Karypis G, Kumar V. Multilevel *k*-way partitioning scheme for irregular graphs. *Journal of Parallel and Distributed Computing* 1998; **48**:96–129.
10. http://www-users.cs.umn.edu/ karypis/metis/.
11. Razavi AH. *ArcView GIS/Avenue Developer's Guide*. Onword Press: USA, 1999.
12. Razavi AH, Warwick V. *ArcView GIS/Avenue Programmer's Reference*. Onword Press: USA, 1999.
13. Taniguchi T, Yamashita Y. Mesh generation of arbitrary 3-dimensional body using only nodes on its surface. *Proceedings of GAMM-Seminar Leipzig 2001*, 2001; 121–133.
14. Ohya Y, Ozono S, Matsuo K, Maeda A. Stratified flow over a 2-D semicircular cylinder in fluid of finite depth. *Proceedings of 12th Symposium on Wind Engineering*, 1992; 13–18 (in Japanese).

